ELSEVIER

Journal of Alloys and Compounds 239 (1996) 71–76

Journal of ALLOYS AND COMPOUNDS

Short-range order of yttria doped zirconia powders studied by X-ray absorption (II)

L. Esquivias[a], C. Barrera-Solano[a], M. Piñero[a], C. Prieto[b]

[a] *Departamento de Física de la Materia Condensada, Facultad de Ciencias, Universidad de Cádiz, Apartado 40, Puerto Real, 11510 Cádiz, Spain*

[b] *Instituto de Ciencias de Materiales de Madrid, Consejo Superior de Investigaciones Científicas, Facultad de Ciencias, Universidad Autónoma, 28049 Madrid, Spain*

Received 18 November 1995; in final form 10 February 1996

Abstract

The atomic structure of polymorphic zirconia powders doped with 6 mol.% yttria prepared by controlled hydrolysis of alkoxides has been studied by X-ray absorption spectroscopy. The short-range orders before and after heat treatment have been compared. The crystallization and incorporation of the yttrium atoms into the network have been monitored. Rietveld analysis of X-ray diffraction data has been used to determine the relative amounts of crystalline phases present in the sample.

Keywords: Yttria stabilized zirconia; X-ray absorption; Structure; Powders; Sol-gel processes

1. Introduction

The outstanding mechanical performance of yttria doped zirconia arises from the transformation from the tetragonal to the monoclinic phase caused by the stress field around a crack, known as martensitic transformation. Monoclinic zirconia (herein m-ZrO_2) grains, occupying more volume than tetragonal ones (t-ZrO_2), press the crack tip, preventing its propagation. Monophase t-ZrO_2 is formed for a 3 mol.% Y_2O_3 content. Between 3 and 6 mol.% a tetragonal phase coexists with the cubic phase (c-ZrO_2) which is stable. For yttria content higher than 6 mol.% zirconia is fully stabilized. Anyway, not all the tetragonal crystallites are able to undertake martensitic transformation under external stresses, even when subjected to intense milling. This type of tetragonal phase, called "non-transformable" tetragonal (t'-ZrO_2), appears after heat treatment for certain cooling conditions and initial structure [1,2]. The yttria content of t'-ZrO_2 is higher than that of t-ZrO_2. It has a structure very similar to that of the cubic phase, the unit cell just presenting a slight distortion from the cubic unit cell. That is why this variant is also called pseudo-cubic.

Thus, for low Y_2O_3 content, a homogeneous distribution of the dopant is critical for a satisfactory behaviour. X-ray diffraction is insufficient to provide information about the dopant and host cation distribution because it only discerns long-range structural features. In multiphase materials, overlapping diffraction peaks could hinder a knowledge of which phases are present in what amounts. In these cases, Rietveld analysis is convenient for evaluating the relative amount of each phase. X-ray absorption spectroscopy (XAS) has also proved useful for such a study because it is a short-range probe sensitive to very low dopant concentration.

In a previous paper [3], we have presented results on yttria doped zirconia powders prepared by co-precipitation of $ZrOCl_2 \cdot 8H_2O$ and pure yttria. The three zirconia polymorphs coexist in the powders prepared in this way and the distribution in the zirconia lattice is inhomogeneous. Hydrolysis and polycondensation of alkoxides [4] is a plausible method for obtaining highly pure and easily sinterable powders once a total elimination of the unwanted organic residues has been completed. The most frequently claimed characteristic of the sol-gel process is that this technique guarantees homogeneity at a molecular level. However, commercial alkoxides are expensive and sometimes difficult to find. Only an optimum reliability of the solid solution powders

PII S0925-8388(96)02267-0

prepared by this method would make its use advisable. In the present paper, analysis of the X-ray absorption results of yttria doped zirconia powders prepared by alkoxide controlled hydrolysis is discussed.

2. Experimental procedures

2.1. Powder preparation and relative phase content determination

6 mol.% yttria doped zirconia was obtained from controlled hydrolysis of $Zr(^nC_3H_7O)_4$ and $Y(^iC_3H_7O)_3$ [4], based on the technique of Fegley et al. [5], in a specially designed device as described elsewhere [6]. The dry powders were subjected to oxidation treatment at 350 °C followed by calcination at 600 °C. Samples are referred to as "xMC". $x = 1$ indicates as-prepared and $x = 2$, heat treated at 600 °C. The actual Y_2O_3 content was 7.1 ± 0.9 mol.%, checked by X-ray energy dispersion in a Jeol JSM-820 scanning electron microscope. 1C and 2C refer to the respective counterparts described in our former paper.

X-ray diffraction (XRD) patterns were obtained with Cu Kα_1 and Cu Kα_2 radiations ($\lambda_1 = 0.1541$ and $\lambda_2 = 0.1544$ nm respectively), selected by means of a graphite monochromator situated behind the sample. The working conditions were 40 mA and 40 kV. Data were collected in the interval $10° < 2\theta < 90°$ with a step size of $\Delta(2\theta) = 0.015°$. Counts of each step were measured for 1 s. The relative amounts of crystalline phases present in the samples were determined by Rietveld analysis of the X-ray diffraction (Philips PW 1830 at the Servicios Centrales de Ciencia y Tecnología de la Universidad de Cádiz, Spain). The data fitting was carried out by means of FULLPROF software [7]. This program allows multiphase analysis of diffraction spectra using the space group and cell parameters of the phases involved as starting structural information. Silicon was used as a reference for Rietveld analysis [8]. The goodness of fit is given by the usual agreement parameters [9].

2.2. X-ray Absorption Spectroscopy

XAS measurements were made at room temperature using the fast-EXAFS acquisition operative mode [10] on beam-line XAS3 at D.C.I. storage ring (Orsay, France). The experimental and EXAFS data analysis procedures were the same as those described in part I of this paper, also the X-ray absorption near edge structure (XANES) spectra.

XANES was interpreted qualitatively on the basis of empirical ideas. To evaluate neighbouring positions around the absorber atoms, the well-known theoretical EXAFS function $\chi(k)$ in the single scattering theory and in the plane-wave approximation was used [11]. We reproduce it here just for convenience:

$$\chi(k) = \sum_j \frac{N_j}{R_j^2} \exp(-2k^2\sigma_j^2) \exp\left(\frac{\Gamma_j R_j}{k}\right) f_j \times \sin[2kR_j + \varphi_j(k)] \quad (1)$$

where

$$k = \left[\frac{2m_e}{\hbar^2}(E - E_0)\right]^{1/2}$$

is the photoelectron wave vector modulus, m_e being the electron mass and E_0 the threshold energy. As usual, an approximate energy value near the edge (E_{0i}) was initially assigned to $k = 0$. Then, during fitting, $\Delta E_0 = E_0 - E_{0i}$ is treated as an additional parameter. N_j is the average coordination number for the Gaussian distribution of distances centred at R_j. σ_j is the Debye–Waller contribution, $\varphi_j = 2\delta(k) + \gamma_j(k)$ is the phase shift, $\delta(k)$ and $\gamma_j(k)$ being those of the central and backscattering atoms respectively. f_j is the amplitude of the backscattering atoms, $\Gamma_j = k/\Lambda(k)$, $\Lambda(k)$ being the photoelectron mean free path. To estimate the shift caused by the scattering phase [12] $f_j(k)$ and $\varphi_j(k)$ have been theoretically calculated by the method reported by Rehr et al. [13], which includes a calculation of $\Lambda(k)$. To avoid spurious oscillations Fourier transforms Rehr et al. [13], which includes a calculation of $\Lambda(k)$. To avoid spurious oscillations Fourier transforms FT were calculated with a Hanning window, selecting the transform range 3 to 13 Å. The FT of $k^3\chi(k)$ is the pseudo-radial distribution function (PRDF). Data have been fitted in the k- and R-spaces by comparison of experimental data (filtered to extract the EXAFS contribution of the coordination sphere) and spectra calculated by Eq. (1). As in our former paper, we have used initially the reported structural parameters [14–21]. A model with more than one shell was not necessary in any case because a fit much better than single distance fitting was not obtained.

3. Results

Before calcination, the powder XRD pattern presented the characteristic broad peaks of amorphous materials. After calcination, peaks corresponding to tetragonal and cubic polymorphs were detected (Fig. 1).

The difference between the calculated and experimental profiles, as well as the Bragg reflection of the phases used for the Rietveld analysis, are shown in Fig. 1. The best agreement parameters of the Rietveld analysis resulted when cubic and tetragonal transformable and non-transformable phases were included,

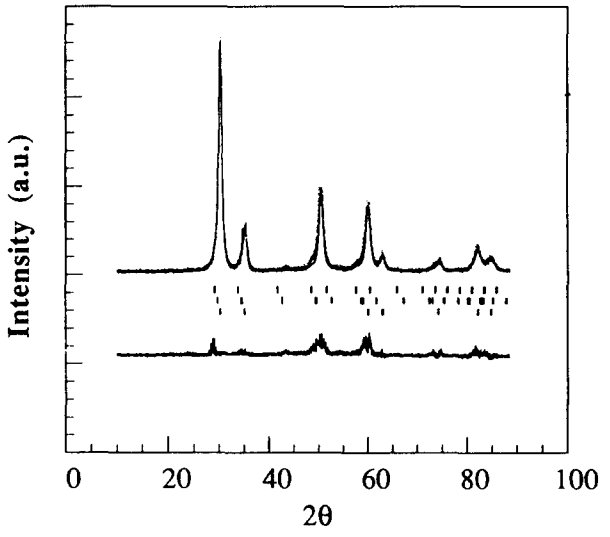

Fig. 1. Experimental intensities (dots) of the sample calcined at 600 °C, X-ray diffraction pattern calculated by Rietveld method (continuous line) and difference between them (bottom). Lines represent the reflection of the phases used for fitting, t-ZrO_2 (top), t'-ZrO_2 (middle) and c-ZrO_2 (bottom).

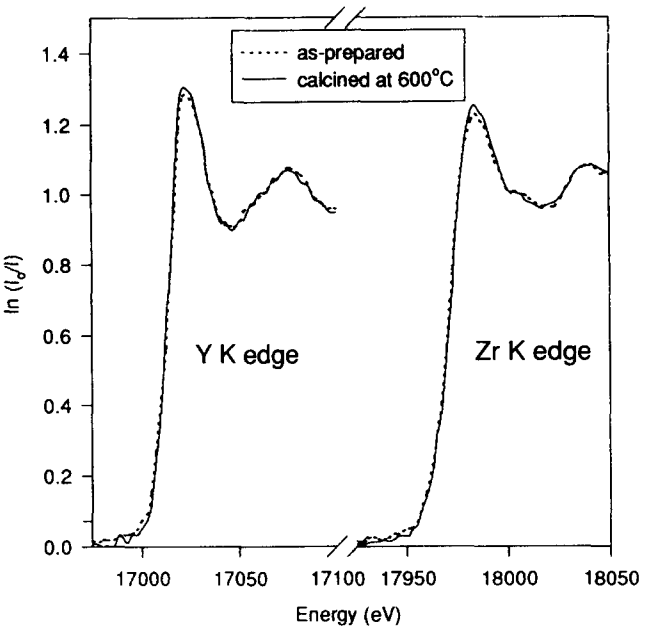

Fig. 2. Room temperature XANES spectra of Zr K-edge (right) and Y K-edge (left) for as-prepared and calcined zirconia powders doped with 6 mol.% yttria.

using as reticular constant starting values and space groups those described in the literature [22–24]. In contrast to the sample described in paper I, no reflections characteristic of the monoclinic phase were observed in the experimental pattern. The percentages of each phase are listed in Table 1. Small changes in the working conditions, e.g. cooling rate, could lead to appreciable alterations of the relative amounts. This means that only the overall values of relative phase amounts have a structural meaning (Table 1).

The XANES spectra are represented in Fig. 2 and their first derivative in Fig. 3. Zr K-edge spectra do not show any remarkable difference with regard to their counterpart samples prepared by coprecipitation of $ZrOCl_2 \cdot 8H_2O$ and pure yttria [3]. The feature at about 10 eV from the edge threshold, attributed to a distortion from centrosymmetry [25–27], is observed in the Zr K-edge spectrum of 2MC but not in the spectrum of 1MC. As in the 2C sample described in our former paper, this confirms that 2MC counterpart contains a tetragonal phase. The splitting of the main peak and a third feature, located 30 eV after the edge, increase with Y concentration [28]. No noticeable changes regarding these features are observed after heat treatment, contrary to what happens with the sample prepared from $ZrOCl_2 \cdot 8H_2O$.

The absorption signal on the Y K-edge of the calcined sample is very similar to that of its respective sample reported in paper I. This is unlike what is observed for the 1MC sample, in which the second oscillation is quite different from that of its counterpart, indicating a different local arrangement. Similar XANES spectra at the Y K-edge are observed in calcined and as-prepared samples, suggesting similar local structures.

Fig. 4 illustrates the PRDF of 1MC and 2MC signals. The peak width and height change significantly, but the first peak position varies by ±2% when distinct types of window with different width are used.

For the fitting we have followed the same strategy and start values as those described in the previous paper. The fits obtained in real space are represented in Figs. 5 and 6. Table 2 list the values used in Fourier filtering and the structural data resulting from the fitting.

Table 1
Percentages of each phase obtained by Rietveld analysis

Phase	wt. %
t-ZrO_2	38
c-ZrO_2 + t'-ZrO_2	62

4. Discussion

A striking characteristic of the PRDF of 1MC (Fig. 4) is the existence of the peak corresponding to the cation–cation distance, which is almost nonexistent in that of 1C [3]. Both O–cation shells have similar amplitudes, while the Y–cation shell is larger and higher than the Zr–cation shell. This indicates that the local order around Zr atoms in 1MC shows features of yttria doped zirconia, except for the bond length. The Y atoms have already merged with the zirconia network. Thus, the zirconia network in the sample pre-

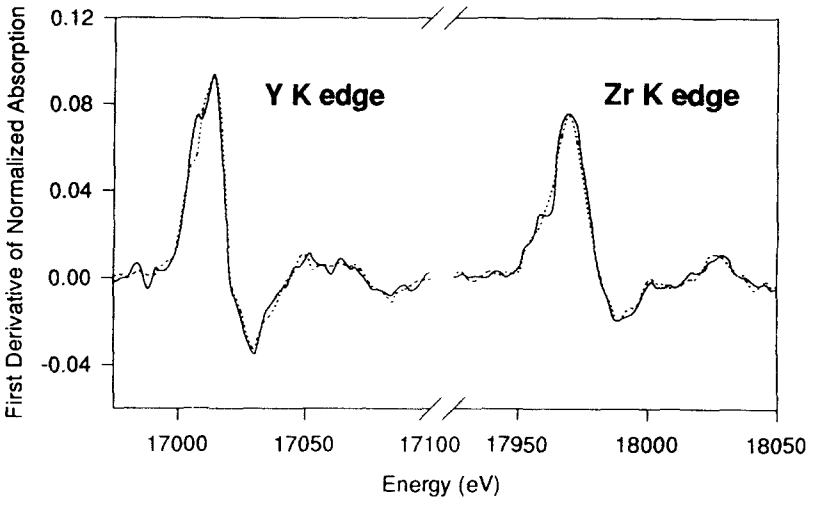

Fig. 3. First derivative of Y and Zr K-edges for as-prepared (dotted line) and calcined (continuous line) zirconia powders doped with 6 mol.% yttria.

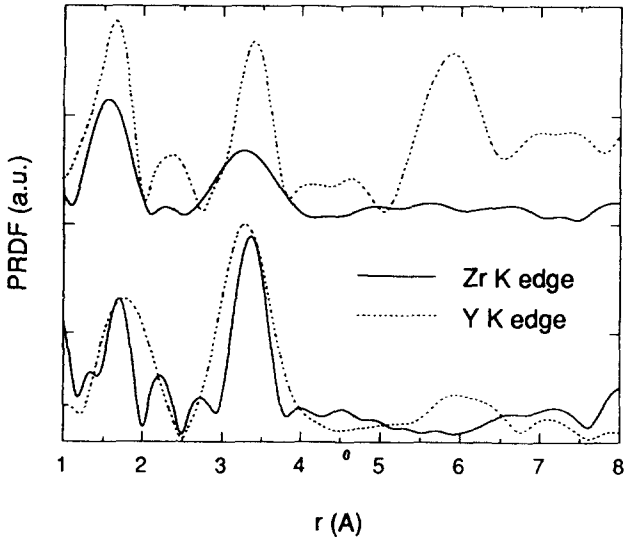

Fig. 4. Fourier transform of Zr and Y $k^3\chi(k)$ weighted signals for as-prepared (bottom) and calcined (top) zirconia powders doped with 6 mol.%.

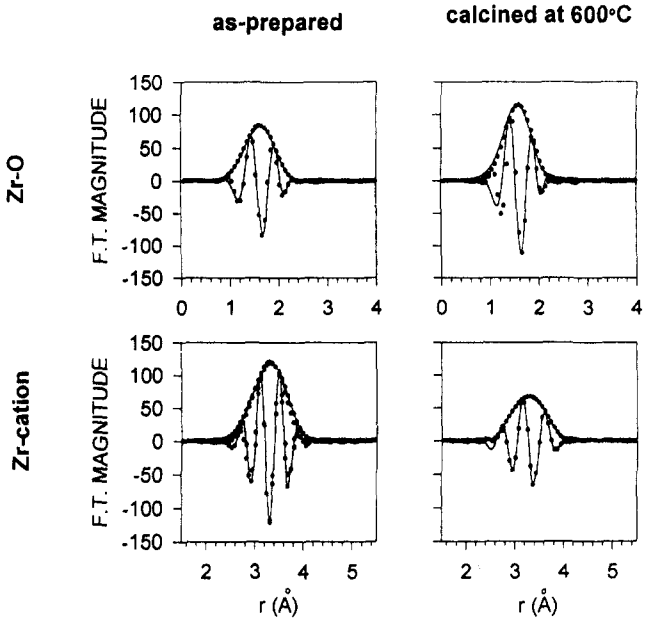

Fig. 5. Comparison of experimental (points) with calculated (continuous lines) modulus and imaginary part of the filtered EXAFS data in R-space at the Zr K-edge. Zr–O shell (top) and Zr–cation shell (bottom) of the as-prepared (left) and calcined (right) samples.

pared from alkoxides is formed from the very beginning of the process. The first peak amplitude of the Y K-edge PRDF of sample 1MC is lower and the peak is broader than that of its 2MC counterpart, as can be expected for an amorphous sample. The Y–O bond length is 4% larger than in Y_2O_3 and yttria doped zirconia. [28]. This is also very near to the Shannon distance for eight-fold coordination and, owing to the amorphous character of this sample, larger than that calculated in several solid solutions (2.33 Å). The difference here is huge with respect to the samples described in paper I. In the sample prepared from alkoxides the value of the Debye–Waller factor indicates that the arrangement around the Y atoms is not as chaotic as in the previous case. The peak of the second neighbours fits 3.63 Å (×12), almost like the crystalline polymorphs. The amorphous sample presents a first peak lower than the second one, as in the samples with tetragonal phase content. The tetragonal phase consists of a two-shell structure of ZrO_8 units, and the outer Zr–O subshell with four Zr–O bonds [29] cannot be seen at room temperature because it corresponds to loose Zr–O bonds. They contribute only to a broad background of the X-ray absorption spectrum. This accounts for the four-fold coordination that the best fit to the Zr–O shell gives, in spite of the long Zr–O bond distance (2.20 Å).

With regard to the calcinated sample, the first peak

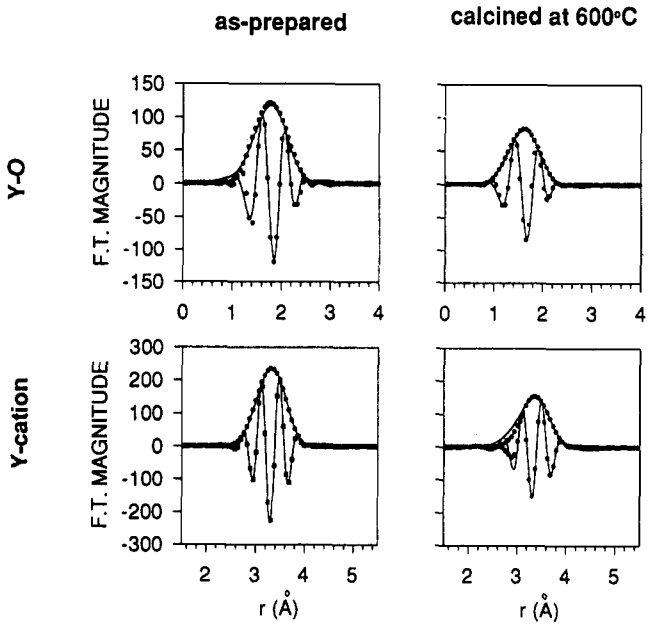

Fig. 6. Comparison of experimental (points) with calculated (continuous lines) modulus and imaginary part of the filtered EXAFS data in R-space at the Y K-edge. Y–O shell (top) and Y-cation shell (bottom) of the as-prepared (left) and calcined (right) samples.

of the Zr edge PRDF has a larger magnitude than the second one. This was also observed in the sample prepared from $ZrOCl_2 \cdot 8H_2O$, but to a lesser extent. Ping-Li et al. [28–30] in their study on XAS of zirconia polymorphs showed that the effect of Y_2O_3 dopant on the Zr K-edge PRDF lowers the second peak amplitude. This is accompanied by an increase in the first peak amplitude. The second peak amplitude decreases with increasing cubic phase concentration as a consequence of the atomic disorder of stabilized *c*-zirconia [28]. The calculated bond distance in the calcined sample is very near to the expected distance of 2.33 Å and considerably shorter than the values reported for its counterpart in paper I, for which a two-shell model gave a much better fit than the single distance fitting. It is worth noting that a single shell model fits the Y–cation peak. It is at this level that major structural differences with the sample prepared by coprecipitation can be observed, because a three-shell model was necessary to fit that peak.

The Zr–cation peak is defined well enough to estimate the second neighbour distance at 3.62 Å, although a low coordination results because of the same reason stated for the first coordination sphere. These values do not represent a deviation from the values reported for yttria stabilized cubic zirconia (12×3.62 Å). For a comparison with the sample prepared by coprecipitation, it must be stated that only a two-shell mode fitted properly the 2C Zr–cation peak. The Zr–O bond length agrees with the reported results. The best fit to the Zr–O shell of the calcined sample gives a shorter bond length (2.11 Å) and five-fold coordination. This bond length agrees with what must be expected for a mixture of tetragonal and cubic phases, that is, a value near the bond length of the majority phase. The low coordination number obtained also denotes a mixture of cubic and tetragonal phases, since the cubic phase is formed by seven-fold coordinated Zr atoms. The resulting coordination number agrees with the phase content obtained by Rietveld analysis, permitting an error in N_{CN} of as much as 20%.

The good distribution of yttria through the zirconia is evidenced by back-transforming the second shell contributions (Fig. 7). No remarkable differences between the second shells of both cations are observed. This implies a considerable homogeneity, since one of the characteristics of zirconia with low yttria concentration is that the atomic arrangements around Zr and Y at the second nearest neighbour level are indistinguishable.

5. Conclusions

Controlled hydrolysis of alkoxides allowed us to prepare zirconia–yttria solid solutions in which Y atoms are in the ZrO_2 lattice from the very beginning of the process. This is already evidenced in the as-

Table 2
EXAFS results of zirconia powders doped with 6 mol.% yttria

Edge	Sample	Bonding	ΔR (Å)	Δk (Å^{-1})	N_{CN}	R (Å)	σ^2 (Å^2)	ΔE_0 (eV)	ε^* (%)
Zr	as-prepared	Zr–O	1.2–2.0	3.0–11.0	4	2.20	0.0104	−10	22.8
	as-prepared	Zr–cation	2.6–3.9	3.0–11.5	4	3.62	0.0046	0.30	88.1
	calcined	Zr–O	1.2–2.1	3.0–11.5	5	2.11	0.0100	−10	71.8
	calcined	Zr–cation	2.8–3.8	3.0–11.2	12	3.62	0.0190	9.2	25.4
Y	as-prepared	Y–O	1.3–2.3	3.0–11.0	8	2.42	0.0096	−1.5	52.3
	as-prepared	Y–cation	2.7–3.9	4.9–11.2	12	3.63	0.0094	−1.5	84.4
	calcined	Y–O	1.4–2.1	3.0–11.0	8	2.35	0.0085	1.0	35.5
	calcined	Y–cation	2.8–3.9	3.0–13.0	12	3.64	0.0128	−1.2	61.7

* $\varepsilon = \Sigma (k^2\chi(k)_{exp} - k^3\chi(k)_{calc})^2 / \Sigma (k^3\chi(k)_{exp})^2$.

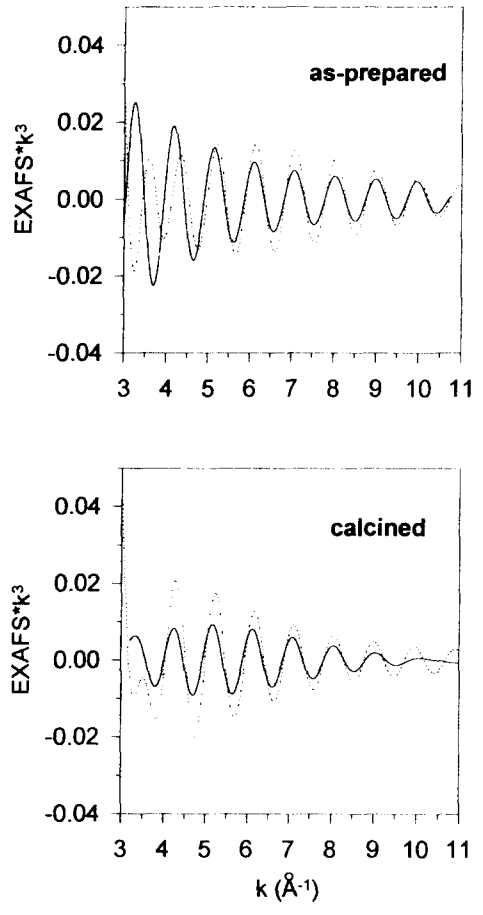

Fig. 7. EXAFS spectra for the Zr–cation (continuous line) and Y–cation (dotted line) shells. The Y–cation signal is deliberately shifted to match that of the Zr–cation.

prepared powders, where Y atoms are already in the zirconia network, contrary to results for powders prepared by coprecipitation [3]. This is manifested by the presence of a second neighbour peak in the PRDF found at the same R_2 around both cations. In the crystallized powders, t-ZrO_2 and c-ZrO_2 + t′-ZrO_2 coexist in a weight ratio of about 2:3. This indicates that, although Y_2O_3 is not thoroughly distributed, the homogeneity is much higher than that of the powder studied in the former paper. It is therefore worth initiating a study on the sintering behaviour and mechanical performance of bulks prepared from these powders.

Acknowledgements

The authors thank the staff in charge of the D.C.I. machine for beam time allocation. We acknowledge the CICYT (Project MAT94-0120-C03), Junta de Andalucía (Exp. No. 6015) and the Ministerio de Eduación y Ciencia for the financial support of this work.

References

[1] R.H.J. Hannik and R.C. Garvie, *J. Mater. Sci., 17* (1982) 2637.
[2] V. Lanteri, A.H. Heuer and T.E. Mitchell, in M. Rhüle, N. Calussen and A.H. Heuer (Eds.), *Science of Zirconia II, Advances in Ceramics*, Vol. 12, The American Ceramic Society, Columbus, OH, 1984, p. 118.
[3] C. Jiménez-Solís, L. Esquivias and C. Prieto, *J. Alloys Comp., 228* (1995) 188.
[4] B. Fegley, Jr. and E.A. Barringer, In C.J. Brinker (Ed.), *Better Ceramics Through Chemistry; Mater. Res. Soc. Symp. Proc. 32*, Elsevier, New York, 1984, pp. 187–197.
[5] B. Fegley, Jr., P. White and H.K. Bowen, *Am. Ceram. Soc. Bull., 64* (8) (1985) 1115.
[6] C. Barrera-Solano, C. Jiménez-Solís, N. de la Rosa-Fox and L. Esquivias, *J. Sol-Gel Sci. Technol., 2* (1994) 347.
[7] J. Rodríguez, M. Anne and J. Pannetirr, in *A System for Time-Resolved Data Analysis (Powder Diffraction Pattern)*, Institute Laue-Langevin (ILL) Int. Rep. 87R014T, 1987.
[8] C. Barrera-Solano, *Ph.D. Thesis*, Universidad de Cádiz, Spain, 1994, pp. 138–141.
[9] S.A. Howard and K.D. Preston, in D.L. Bish and J.E. Porter, *Modern Powder Diffraction*, The Minerological Society of America, p. 217.
[10] C. Prieto, P. Lagarde, H. Dexpert, V. Briois, F. Villain and M. Verdaguer, *Meas. Sci. Technol, 3* (1992) 325.
[11] K. Teo, in *Inorganic Chemistry Concepts 9*, Springer, Berlin, 1986.
[12] A.G. Mckale, B.W. Veal, A.P. Paulikas, S.K. Chan and G.S. Knapp, *J. Am. Chem. Soc, 110* (1986) 3763.
[13] J.J. Rehr, J. Mutree de León, S.I. Sabinsky and R.C. Albers, *J. Am. Chem. Soc., 113* (1991) 5135.
[14] D.K. Smith and H.W. Newkirk, *Acta Crystallogr., 18* (1965) 983.
[15] O. Othaka, T. Yamanaka, S. Ku, N. Hara, H. Asano and F. Izumi, *Proc. Jpn. Acad. B, 66* (1990) 34.
[16] G. Teufer, *Acta Crystallogr., 15* (1962) 1187.
[17] P. Alderbert and J.P. Traverse, *J. Am. Ceram. Soc., 68* (1985) 34.
[18] D. Michel, L. Mazerolles and M. Pérez y Jorba, *J. Mater. Sci., 18* (83) 2618.
[19] D. Steele and B.E.F. Fender, *J. Phys. C, 7* (19XX).
[20] D.K. Smith and C.F. Cline, *Am. Ceram. Soc., 45* (1962) 249.
[21] A.N. Christensen, R.G. Hazell and Å. Nilsson, *Acta Chem. Scand., 21* (1967) 481.
[22] G. Taufer, *Act. Crystallogr., 15* (1982) 1187.
[23] D.K. Smith and H.W. Newtik, *Act. Crystallogr., 18* (1965) 983.
[24] D.K. Smith and C.F. Cline, *J. Am. Ceram. Soc., 45* (1962) 249.
[25] J. Frandon, B. Brousseau and F. Pradal, *Phys. Status Solidi B 98* (1980) 379.
[26] A.L. Roe, D.J. Scaneider, R.J. Mayer, J.W. Pyrz, J. Widom and L. Que, Jr., *J. Am. Chem. Soc., 106* (1984) 1676.
[27] J.E. Hahn, R.A. Scott, K.O. Hodgson, S. Doniach, S.R. Desjardins and E.I. Solomon, *Chem. Phys. Lett., 39* (1982) 595.
[28] Ping-Li, I.-Wei Chen and J.E. Penner-Hahn, *Phys. Rev. B, 48* (14) (1993) 10074.
[29] Ping-Li, I.-Wei Chen and J.E. Penner-Hahn, *Phys. Rev. B, 48* (14) (1993) 10063.
[30] Ping-Li, I.-Wei Chen and J.E. Penner-Hahn, *Phys. Rev. B, 48* (14) (1993) 10082.